




# Anisotropy reduction of additively manufactured AlSi10Mg for metal mirrors

Songnian Tan<sup>1,2,3</sup>, Yefei Wang<sup>1,2,3</sup>, Weiyi Liu<sup>1,3</sup>, Hao Wang<sup>1,3</sup>, Ping Jia<sup>1,3</sup>, and Yalin Ding<sup>1,3,\*</sup> 

<sup>1</sup> Changchun Institute of Optics, Fine Mechanics and Physics, Chinese Academy of Sciences, 3888 Southeast Lake Road, Changchun 130033, China

<sup>2</sup> University of Chinese Academy of Sciences, Yuquan Road, Beijing 100049, China

<sup>3</sup> Key Laboratory of Airborne Optical Imaging and Measurement, Chinese Academy of Sciences, 3888 Southeast Lake Road, Changchun 130033, China

**Received:** 9 November 2021

**Accepted:** 3 March 2022

**Published online:**  
13 May 2022

© The Author(s), under exclusive licence to Springer Science+Business Media, LLC, part of Springer Nature 2022

## ABSTRACT

In light of the rapid development of additive manufacturing technologies, this study explores the additive manufacturing of an AlSi10Mg mirror for potential application in aerospace engineering. An additively manufactured mirror consisting of AlSi10Mg must demonstrate high-dimensional stability to maintain its surface accuracy. This study investigates the origin of the anisotropy of AlSi10Mg, fabricated by selective laser melting (SLM), by analyzing its microstructure using metallographic microscopy and scanning electron microscopy. The microstructure of AlSi10Mg fabricated by SLM is analyzed relative to the build and scan directions. In addition, the effect of heat treatment on the microstructure, inherent anisotropy, tensile strength, elongation, hardness, and thermal expansion of AlSi10Mg fabricated by SLM is studied. Heat treatment effectively reduces the inherent anisotropy of AlSi10Mg fabricated by SLM. Moreover, the surface accuracy of a heat-treated, additively manufactured mirror consisting of AlSi10Mg is stable, that is, minimally affected by thermal cycling. This study can inform further research on dimensionally stable, additively manufactured AlSi10Mg parts and the development of metal mirrors.

## Introduction

Additive manufacturing (AM) is a fabrication approach favored by researchers in the field of aerospace engineering because of advantages such as

rapid prototyping, high forming accuracy, and design freedom in terms of the complexity of the shapes of parts [1]. AlSi10Mg is an aluminum alloy most commonly used in selective laser melting (SLM)

Handling Editor: M. Grant Norton.

Address correspondence to E-mail: dingyalin@ciomp.ac.cn

in AM technology [2]; it can be used to prepare optical components such as aerospace mirrors [3, 4].

The fabrication of these mirrors involves the formation of mirror substrates by the SLM of AlSi10Mg powder [5]. The suitability of a material for application in additively manufactured metal mirrors is determined by its mechanical properties; in particular, its dimensional stability determines whether it can be used in optoelectronic devices. The substrate of an aerospace mirror is required to be dimensionally stable in a wide temperature range in order to maintain its surface accuracy. Thus, to use additively manufactured AlSi10Mg as a substrate for an aerospace mirror, it must be dimensionally stable.

The main factors affecting the dimensional stability of additively manufactured AlSi10Mg parts are:

- (1) Residual stress within additively manufactured AlSi10Mg parts. During the AM of a part (such as a mirror substrate), a high-temperature gradient causes transient thermal deformation in the area subjected to SLM. Once the laser departs from the melted area, continuing its scan, the temperature of this area of the processed part decreases rapidly, causing significant shrinkage relative to the surrounding area [6] and resulting in residual stress. A change in the ambient temperature can release this residual stress, affecting the surface accuracy of the part (mirror substrate).
- (2) Anisotropy of additively manufactured AlSi10Mg parts [7]. Additively manufactured AlSi10Mg parts consist of stacked metal layers that are formed by the SLM of AlSi10Mg powder. Consequently, the mechanical properties and thermal dimensional stability of the formed matrix in the scan direction are different from those in the build direction. Additively manufactured AlSi10Mg parts are characterized by anisotropic mechanical properties. Moreover, the anisotropy of additively manufactured AlSi10Mg parts may affect subsequent processing [8]. Under low-temperature conditions, anisotropy leads to non-uniform change in the associated part (such as a mirror substrate), affecting its surface accuracy.

Thus, the anisotropy of an additively manufactured AlSi10Mg mirror substrate and its effect on the accuracy of the mirror surface must be considered. To reduce the internal stress, the mirror is usually placed

at a 45-degree angle for 3D printing. Due to the different properties of the XY direction and the Z-direction, specifically, the difference in the thermal expansion coefficient, changes in the temperature cause astigmatism in the mirror. The optical components (mirrors) of devices used in the laboratory operate under constant temperature conditions, and therefore, the thermal stability of the mirror material is not a significant concern. However, the mirrors used in aerospace engineering are required to operate under harsh environmental conditions and tolerate extreme temperature changes; accordingly, the optical components of refractive optical systems must demonstrate dimensional stability within a wide temperature range.

The heat treatment of metal parts is an important process in mechanical engineering. It improves the performance of the part by changing its internal microstructure [9, 10]. AlSi10Mg is a typical hypoeutectic alloy of the Al–Si–Mg system [11], and the heat treatment of the strengthened alloy can improve its mechanical properties [12, 13] and reduce its surface roughness [14]. Therefore, heat treatment is expected to be an effective way to stabilize an additively manufactured mirror substrate consisting of AlSi10Mg.

The detection of anisotropy of AlSi10Mg material has also been researched. Mechanical property testing is the most common testing method, although new methods such as nondestructive ultrasonic evaluation can also accurately test the anisotropy of materials [15]. Because the AlSi10Mg sample needs to be heat treated, permanent deformation may occur when the AlSi10Mg sample is heated to a high temperature (500 °C) and then returned to normal temperature. This is due to thermally induced porosity [16], which causes errors in the test results. To avoid the influence of thermally induced porosity, reasonable selection of 3D printing forming parameters and hot isostatic pressing (HIP) processing of the formed sample to reduce the porosity is applied [17, 18].

This study analyzes the microstructure of additively manufactured AlSi10Mg, fabricated by SLM, relative to the build and scan directions. The change in the anisotropy of AlSi10Mg in these two directions before and after heat treatment is investigated. Moreover, the effect of heat treatment on the tensile strength, elongation, hardness, and thermal stability of AlSi10Mg is assessed. It was found that heat treatment effectively reduces the inherent anisotropy

of AlSi10Mg fabricated by SLM. In addition, the surface accuracy of a heat treated, additively manufactured mirror consisting of AlSi10Mg is stable, that is, minimally affected by thermal cycling. This research is expected to inform the application of additively manufactured AlSi10Mg parts in aerospace optical components.

## Materials and methods

AlSi10Mg spherical powder, with a particle-diameter range of 13–53  $\mu\text{m}$ , and a metal 3D printer (M290, EOS), equipped with an ytterbium fiber laser (400 W), were used to fabricate AlSi10Mg specimens by SLM. The laser power, scanning speed, and laser spot size were 325 W, 1050 mm/s, and 0.09 mm, respectively, and the scan spacing was set to 0.07 mm. The thickness of each layer was 0.03 mm. To reduce the residual stress, the interlayer alternate scanning mode was adopted, and the phase angle was selected as  $67^\circ$ . The microstructures of as-built AlSi10Mg specimens were observed to investigate the origins of their anisotropy. The T6 heat treatment of Al–Si–Mg parts changes their mechanical properties [19–21]. Consequently, AlSi10Mg specimens fabricated by SLM were heat treated, and the microstructures of the as-built and heat-treated AlSi10Mg specimens were compared to determine the effectiveness of heat treatment in reducing the anisotropy of additively manufactured AlSi10Mg. This study used a heat-treatment process (T6-like) similar to the T6 heat treatment of Al–Si–Mg alloys [22].

The T6-like heat treatment involved the following steps:

- (1) HIP. The processing temperature was  $510^\circ\text{C}$ , and the pressure was 102 MPa,  $530 \pm 5^\circ\text{C}$ , held for 2 h.
- (2) Solution heat treatment. Specimens were heated to  $530^\circ\text{C}$  and maintained at this temperature for 2 h.
- (3) Quenching. After solution heat treatment, the specimens were quenched in water for 10 s.
- (4) Uphill quenching. The specimens were then placed in liquid  $\text{N}_2$  for 30 min before submersion in boiling water.
- (5) Age hardening. Finally, the specimens were age hardened at  $177 \pm 5^\circ\text{C}$  for 8 h. Age hardening is required for subsequent processing.
- (6) Temperature cycle treatment. After finishing, heat cycle treatment was applied three times. The temperature range was  $-190^\circ\text{C}$  to  $+160^\circ\text{C}$ , and the temperature change rate did not exceed  $2^\circ\text{C}/\text{min}$ .

To facilitate the investigation of the anisotropic properties of AlSi10Mg fabricated by SLM and the observation of internal defects, cuboid specimens were fabricated with side lengths of 10 mm. To prepare specimens for metallography, their surfaces were finely ground on water-resistant matte paper, polished to smooth using a polisher, and then etched for 30 s using Keller reagent [ $\text{HNO}_3$  (2.5 mL) +  $\text{HCl}$  (1.5 mL) +  $\text{HF}$  (1 mL) +  $\text{H}_2\text{O}$  (95 mL)]. After the acid treatment (etching process), the specimens were immediately rinsed with ultrapure water, washed with alcohol, and dried using a hair dryer. Morphological analysis and qualitative and quantitative analyses of the elemental composition of AlSi10Mg specimens were performed using a metallographic microscope (GX71, Olympus) and a scanning electron microscope (MIRA3, Tescan), respectively.

To evaluate the effect of the T6-like heat treatment on the anisotropy of AlSi10Mg, the tensile strength, elongation, hardness, and thermal stability of as-built and heat-treated AlSi10Mg specimens were investigated.

The mechanical properties of a material directly affect its performance; to assess the tensile strength and elongation of additively manufactured AlSi10Mg, appropriate specimens were subjected to a tensile test. The dimensions of a tensile specimen are shown in Fig. 1.

Hardness is a mechanical property of metal materials that reflects their ability to resist elastic deformation, plastic deformation, and damage; it can also reflect their ability to resist residual deformation [23]. The hardness of additively manufactured AlSi10Mg was determined by assessing the initial and continuous plastic deformation resistance of AlSi10Mg specimens fabricated by SLM. The higher the plastic deformation resistance of a specimen, the higher its strength. Therefore, the hardness of additively manufactured AlSi10Mg specimens reflects their performance in terms of elasticity, plasticity, strength, and wear resistance (durability). The Vickers hardness of

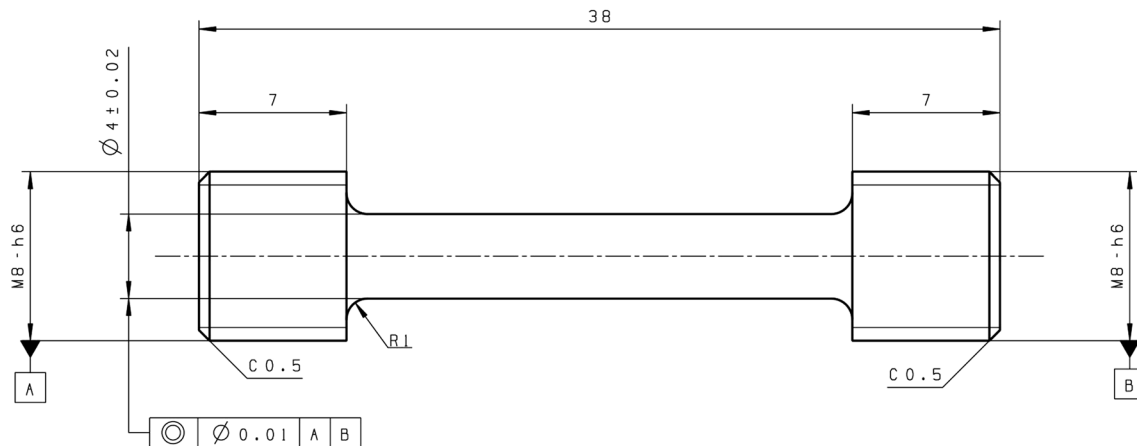


**Figure 1** Illustration of a stretched specimen.

AlSi10Mg specimens was measured using a digital microscopic Vickers hardness tester (HVS21000), which applied a load of 9.8 N for 30 s. The measurement was repeated three times to obtain the average Vickers hardness.

The coefficient of thermal expansion is an important indicator of the thermal stability of additively manufactured AlSi10Mg; it is used to assess the material's suitability for application as an aerospace mirror substrate by quantifying its change in volume under high and low-temperature conditions. The anisotropy of additively manufactured AlSi10Mg also affects its thermal expansion [24]. To accurately quantify the thermal expansion of additively manufactured AlSi10Mg in the build (Z) and scan (X) directions, the linear expansion coefficients of specimens ( $\varnothing 8 \text{ mm} \times 24 \text{ mm}$  in size) were determined using a dilatometer (DIL 402SE, NETZSCH) between  $-50$  and  $70^\circ \text{C}$ .

## Results and discussion

### Microstructure and morphology of as-built AlSi10Mg

The microstructure of an as-built AlSi10Mg specimen, as shown in Fig. 2, is not completely uniform in either the XY or XZ planes. This is owing to the SLM process. However, no obvious pores or hole defects are detected and the metal layers are well connected.

An image (Fig. 2a) of the XY plane of an as-built AlSi10Mg specimen shows a periodic band-like structure, that is, bands delineated by white and bright edges. These are the weld lines formed during

SLM, the overlap area of adjacent melt channels, and remelted zones between layers. Clear boundaries exist between the near-parallel melt channels; moreover, the melt channels have a similar width. During SLM, the width of the strip melt channel is approximately  $180 \mu\text{m}$  and, because the scanning interval is  $110 \mu\text{m}$ , adjacent melt channels overlap by 30–40%. During SLM, elliptical melt channels ensure the compactness of the fabricated part; these form when the laser melts powder next to a recently scanned melt channel resulting in the overlap of melt pools. The temperature at different locations in a melt channel varies, remelting occurs at the overlaps of melt channels, which leads to different compositions and structures at different locations. This phenomenon is highlighted by etching (acid treatment).

An image (Fig. 2c) of the XZ plane of the as-built AlSi10Mg specimen shows the overlaps between melt channels. The surfaces of the observed arches formed by melt channels and overlaps are relatively smooth, which is consistent with the geometry of the melt pool during SLM. The structure is similar in appearance to scaled fish skin, with a “scale” width and thickness of approximately 180 and  $40 \mu\text{m}$ , respectively. This cross section of the overlapping melting channels shows a dense structure [25].

Scanning electron microscopy (SEM) images of the XY plane of an as-built AlSi10Mg specimen are shown in Fig. 3. The laser trajectory is evident in Fig. 3a. The as-built AlSi10Mg specimen is mainly composed of slender columnar  $\alpha\text{-Al}$  dendrites with different growth directions; eutectic Al–Si is present between the dendrites, exhibiting typical epitaxial growth. According to the laser trajectory, the



**Figure 2** Low- (left) and high-magnification (right) metallographic images of an as-built AlSi10Mg specimen showing the overlaps between melt channels in the **a, b** XY and **c, d** XZ planes.

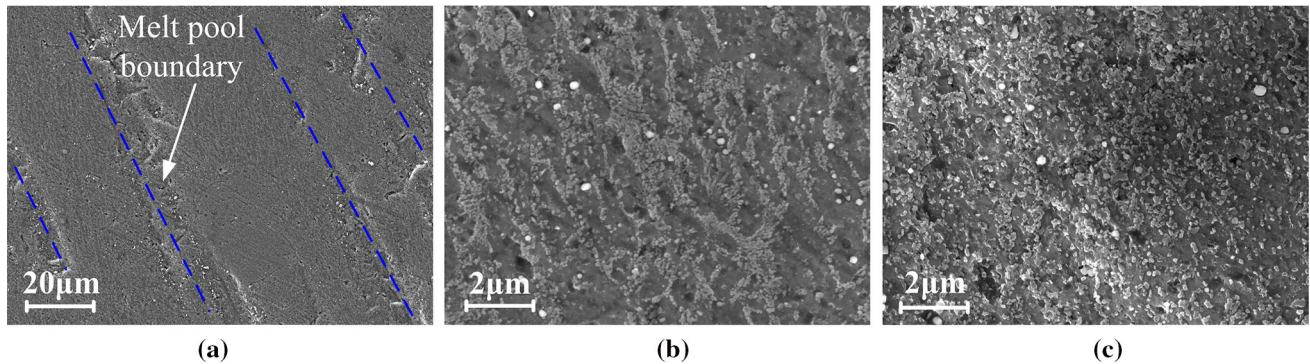
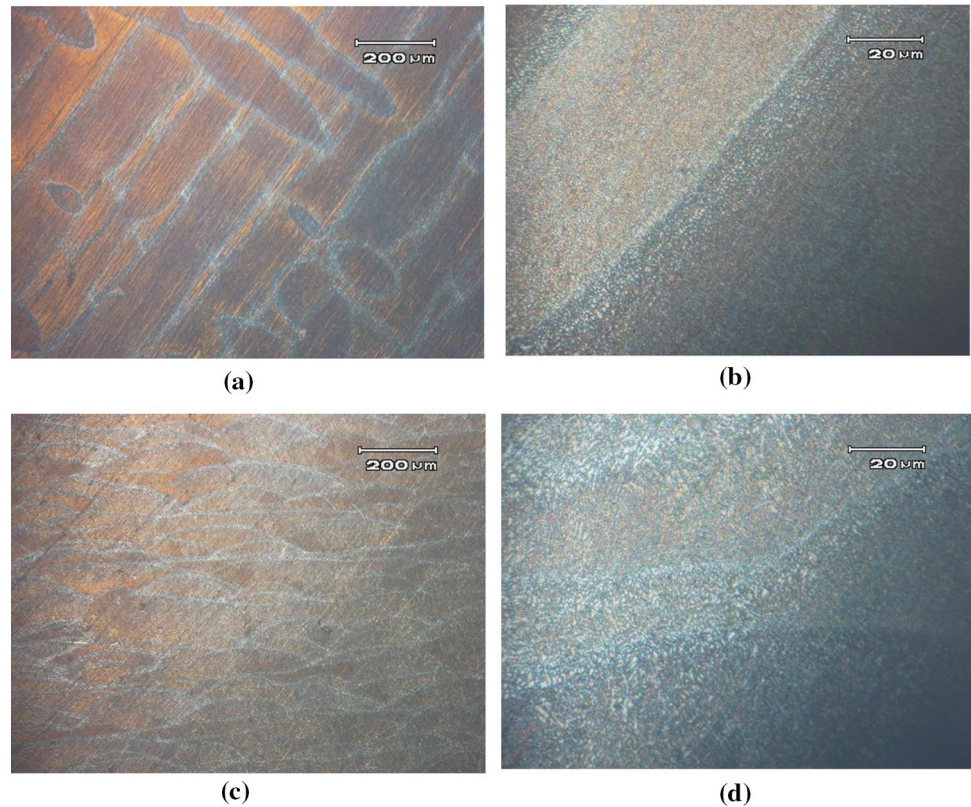


**Figure 3** SEM images of an as-built AlSi10Mg specimen; **a** XY plane, **b** interior of melt channel exhibiting a fine cellular microstructure, and **c** boundary of melt channel exhibiting a coarse cellular microstructure.

structure can be divided into fine-grained and coarse-grained regions. SLM involves the rapid melting (and subsequent rapid solidification) of material using a laser with a low spot diameter (0.11 mm). During SLM, a small melt pool forms with a high cooling rate, which enables the growth of very fine grains in the center of the melt pool; the resulting structure is uniform and dense. Zones that are subjected to remelting, undergo multiple melting and solidification processes which enable further crystal growth. Figure 3b shows the fine-grained region in the center

of a melt channel, featuring fine columnar dendrites, while Fig. 3c shows a coarse-grained region, which is characteristic of the overlap of adjacent melt channels. The morphology of Si in the coarse-grained region differs significantly from its morphology in the fine-grained region. Si no longer forms a continuous network, but forms partially disconnected particles. The crystals observed in the overlaps of melt channels are larger than those in the centers of the melt channels because the overlaps of melt channels

experience two heating (melting) processes, resulting in greater crystal growth.

SEM images of the XZ plane of an as-built AlSi10Mg specimen are shown in Fig. 4. In the build (Z) direction, the as-built AlSi10Mg specimen consists of a network of fine-grained and coarse-grained regions. The small ( $\sim 0.4 \mu\text{m}$ ) gray island-shaped regions are part of the columnar dendritic  $\alpha$ -Al matrix. The white networks are precipitated Si phases in eutectic Al-Si. The Si phases are bright under microscope and form a network within the  $\alpha$ -Al matrix [26]. The coarse-grained region is shown in Fig. 4(c); it likely contains precipitates such as  $\text{Mg}_2\text{Si}$  [27, 28].

Regardless of the observed plane, the as-built AlSi10Mg specimen consists of a high number of fine dendrites. The bright white area indicates that metallurgical bonding occurs between adjacent melt channels and layers. The overall structure appears stable and well fused.

Owing to the structural differences between the XY and XZ planes, and dissimilar distribution of fine and coarse crystals, the mechanical properties of the as-built AlSi10Mg specimen are expected to differ in the build (Z) and scan (X) directions.

The elemental composition of the XZ plane of an as-built AlSi10Mg specimen is shown in Fig. 5. Evidently, Al, Si, and Mg are uniformly distributed, and macrosegregation is not observed. Based on the distribution of Al and Si, the gray island-shaped regions form part of the columnar dendritic  $\alpha$ -Al matrix, while the white networks are precipitated Si phases.

### Microstructure and morphology of T6-like heat-treated AlSi10Mg

Metallographic images of an AlSi10Mg specimen subjected to a T6-like heat treatment are shown in Fig. 6. The structure of the heat-treated AlSi10Mg specimen differs from that of the as-built AlSi10Mg specimen. In the heat-treated AlSi10Mg specimen, eutectic Si precipitate is present in the  $\alpha$ -Al matrix and exists as dispersed round grains. The microstructure of the heat-treated AlSi10Mg specimen is uniform, and there are no obvious microstructural differences between its XZ and XY planes. Dendrites, laser traces, and heat-affected zones are no longer discernable.

SEM images of a heat-treated AlSi10Mg specimen are shown in Fig. 7. The eutectic Si phases exist as dispersed round grains, and their distribution in the XZ and XY planes is approximately uniform. The size of the eutectic Si grains in the heat-treated AlSi10Mg specimen is  $0.2\text{--}2 \mu\text{m}$ .

The elemental composition of a heat-treated AlSi10Mg specimen is shown in Fig. 8. Grains of Si phases are observed in the  $\alpha$ -Al matrix, indicating that the T6-like heat treatment spheroidizes eutectic Si.

Each step of the T6-like heat treatment has a different purpose, but all of these steps aim to achieve isotropy. The additively manufactured metal mirror was processed by HIP to improve its density, and to avoid the influence of thermally induced porosity. The main purpose of solution heat treatment is to spheroidize irregularly shaped eutectic Si particles and dissolve  $\text{Mg}_2\text{Si}$  to form a uniform supersaturated solid solution. Under the action of solution heat treatment, needle-like eutectic Si phases dissolve and

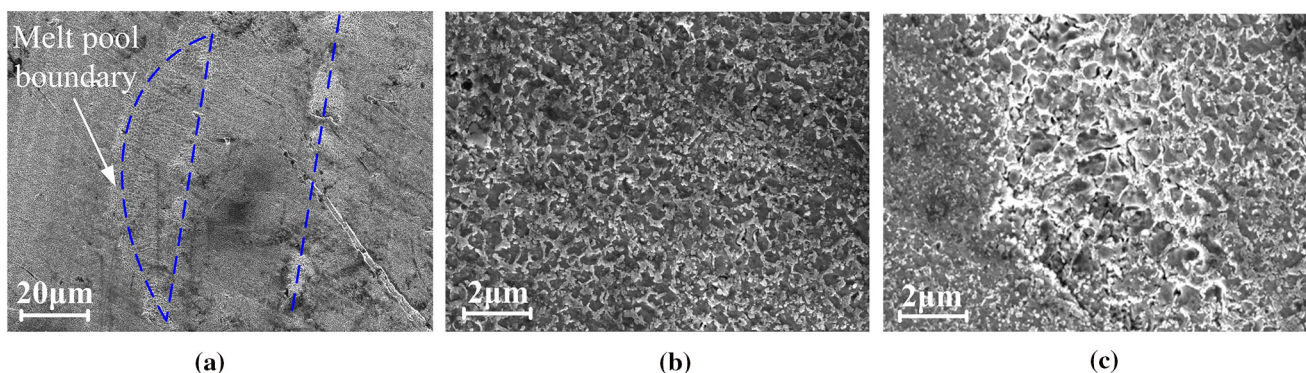


**Figure 4** SEM images of an as-built AlSi10Mg specimen; **a** XZ plane, **b** interior of melt channel with fine cellular microstructure, and **c** boundary of melt channel with coarse cellular microstructure.



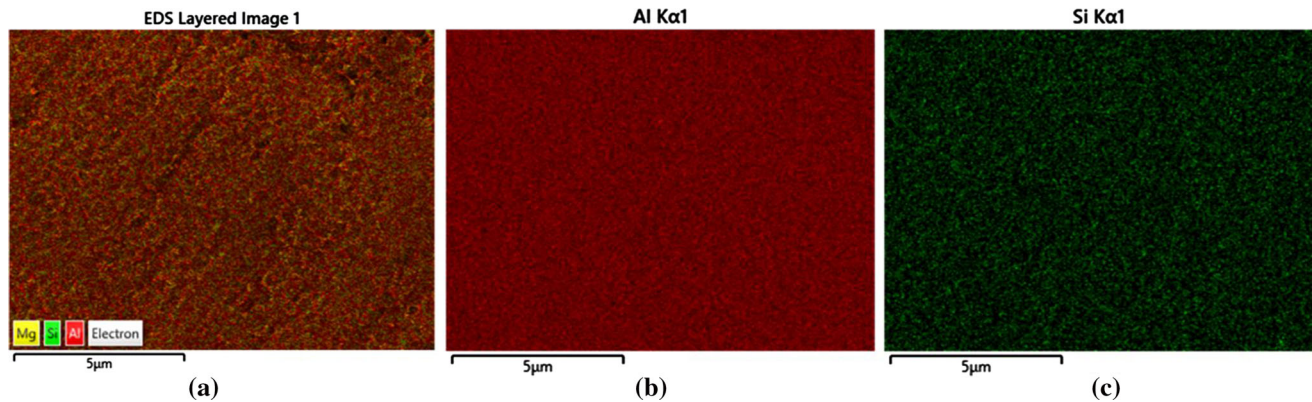
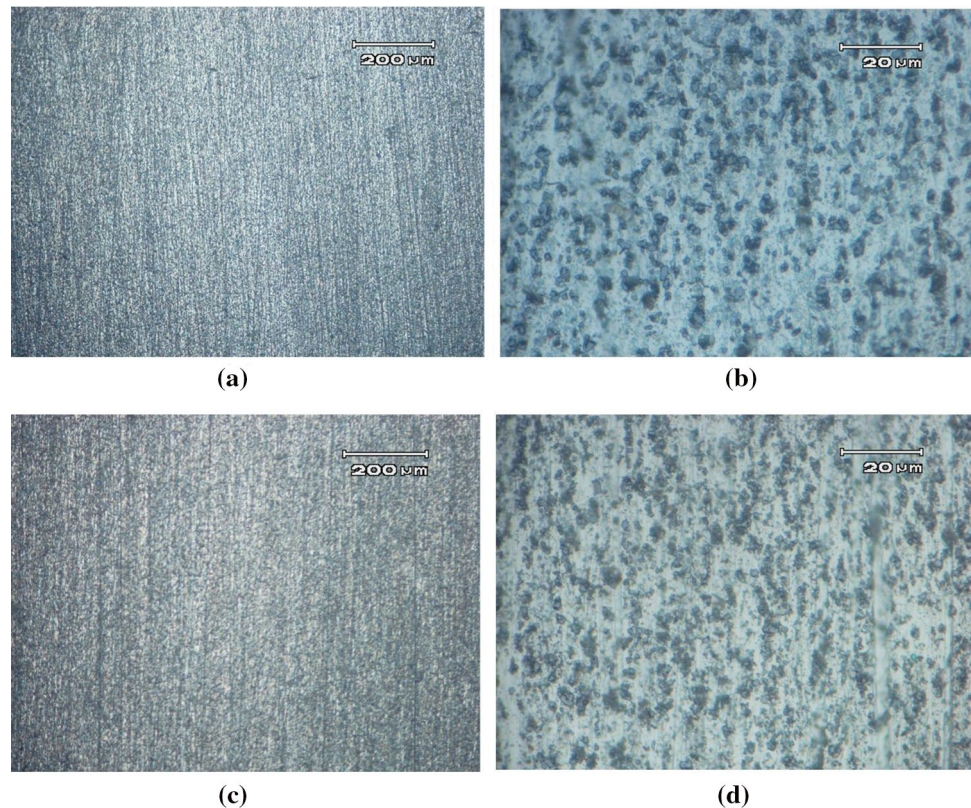


**Figure 5** Elemental composition of an as-built AlSi10Mg specimen; **a** energy dispersive spectroscopy (EDS) map of Mg, Si, and Al, **b** EDS map of Al, and **c** EDS map of Si.

**Figure 6** Low- (left) and high-magnification (right) metallographic images of a AlSi10Mg specimen subjected to a T6-like heat treatment in the **a, b** XY and **c, d** XZ planes.



diffuse at nodes or grooves, breaking into smaller eutectic Si particles. Subsequently, the broken eutectic Si particles granulate and spheroidized under the combined influence of heat/mass diffusion and the curvature effect of the Si/ $\alpha$ -Al interface. The process of transforming coarse and sharp flaky dendrites into fine and approximately circular granular structures proceeds until eutectic Si grains are uniformly distributed to reduce the interface energy and effectively improve the ductility of AlSi10Mg. Adhesion may

occur between adjacent eutectic Si grains. After solution heat treatment, water quenching rapidly reduces the temperature of AlSi10Mg. This process inhibits the formation of precipitation phase and forms supersaturated  $\alpha$ -Al solid solution. Then, uphill quenching is used to counteract the residual stress generated during solution heat treatment. Aging treatments are divided into artificial and natural aging. After uphill quenching, complete artificial aging produces fine and evenly distributed  $\text{Mg}_2\text{Si}$



**Figure 7** Low- (left) and high-magnification (right) SEM images of a AlSi10Mg specimen subjected to a T6-like heat treatment in the **a, b** XY and **c, d** XZ planes.

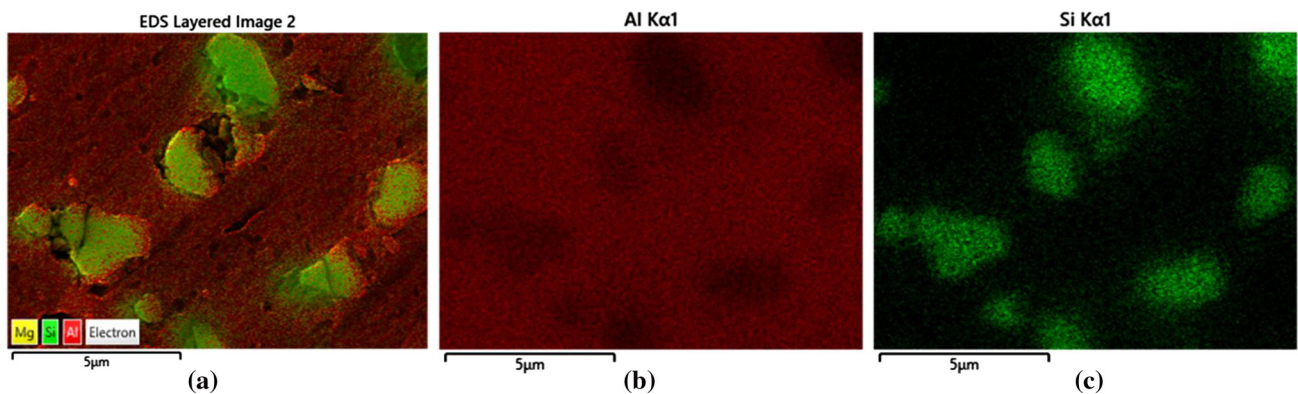
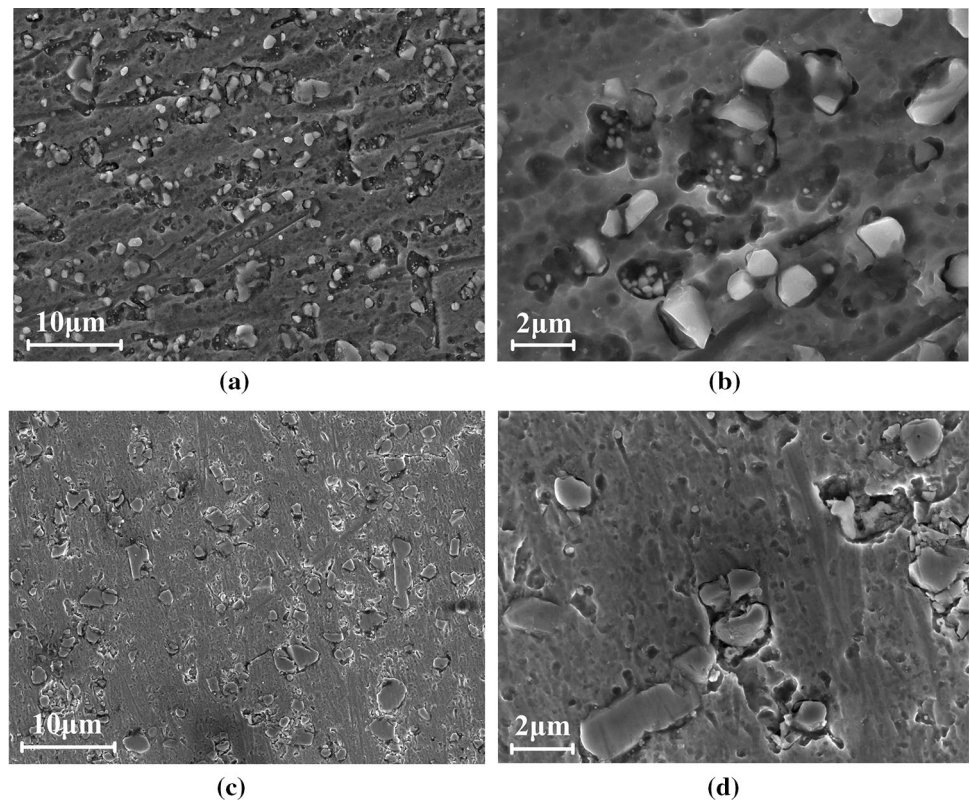


**Figure 8** Elemental composition of a T6-like heat-treated AlSi10Mg specimen; **a** EDS map of Mg, Si, and Al, **b** EDS map of Al, and **c** EDS map of Si.

precipitate and improves the strength of AlSi10Mg. The purpose of the temperature cycle treatment is to repeatedly shrink and expand the alloy, such as the work-body lattice, and make the grains in all directions undergo a small displacement, so as to form the atomic segregation regions and the particles of the metal compound in these solid solution crystalline lattices. This results in a more stable state, improving the dimensional stability of the part.

Annealing heat treatment was also applied to the samples as comparative test, and the heat-treatment

conditions were kept at 180 °C for 8 h followed by air-cooling. The microstructure of the AlSi10Mg sample is in the form of a continuous network (Fig. 9). The eutectic Si phase is partially disconnected, but the network remains, and the microstructure becomes coarser. The original short columnar Si phase in the grains also aggregates and grows. The fine-grained dispersion-strengthening phase begins to precipitate on the gray island-shaped  $\alpha$ -Al matrix.



Both the annealing treatment and the T6 heat treatment can promote the precipitation of Si from the Al matrix in the AlSi10Mg alloy formed by SLM, and the eutectic Si phase on the grain boundary is partially dissolved, fractured, and passivated. However, the annealing treatment cannot effectively improve the anisotropy because the treatment temperature is not high enough. The higher the temperature, the faster the diffusion of Si atoms, so the eutectic morphology of the sample changes drastically during the solid solution stage of the T6 heat treatment (540 °C for 8 h). After T6 heat treatment, the network eutectic Si in the AlSi10Mg alloy formed by SLM was fully dissolved, fractured, and spheroidized. Therefore, the T6-like heat treatment increases the uniformity and isotropy of the internal structure.

The organizational structure of the material determines its mechanical properties. The above analysis of AlSi10Mg fabricated by SLM suggests that its anisotropy is caused by different structural forms. Mechanical properties, which directly affect performance, are an important indicator for measuring materials. To examine the mechanical properties of AlSi10Mg samples before and after heat treatment,

the microhardness, mechanical properties, and thermal expansion coefficient of AlSi10Mg samples were tested.

### Mechanical properties of as-built and heat-treated AlSi10Mg

Tensile mechanical tests were performed on as-built and heat-treated AlSi10Mg specimens at 20 °C; the results are shown in Fig. 10. The as-built AlSi10Mg specimen exhibited the highest tensile strength; however, the strength in the X (467.1 MPa) and Z (438.8 MPa) differs by 6.45%. Its elongation is low; that is, 5.8 and 5.1% in the X- and Z-directions, respectively. Its elongation in the Z-direction elongation is slightly less than that in the X-direction.

The tensile strength of the heat-treated AlSi10Mg specimen is comparatively low, that is, 311.8 and 302.5 MPa in the X- and Z-directions, respectively, which is a difference of 3.17%. The tensile strength of the heat-treated AlSi10Mg specimen is near that of RSA 6061-T6 (318 MPa) [29]. However, its greatly improved elongation of ~ 12% is nearly 1.14 times higher than that of RSA 6061-T6. The difference in the tensile strength of the heat-treated AlSi10Mg

**Figure 9** Low- (left) and high-magnification (right) SEM images of a AlSi10Mg specimen subjected to an annealing heat treatment in the a, b XY and c, d XZ planes.

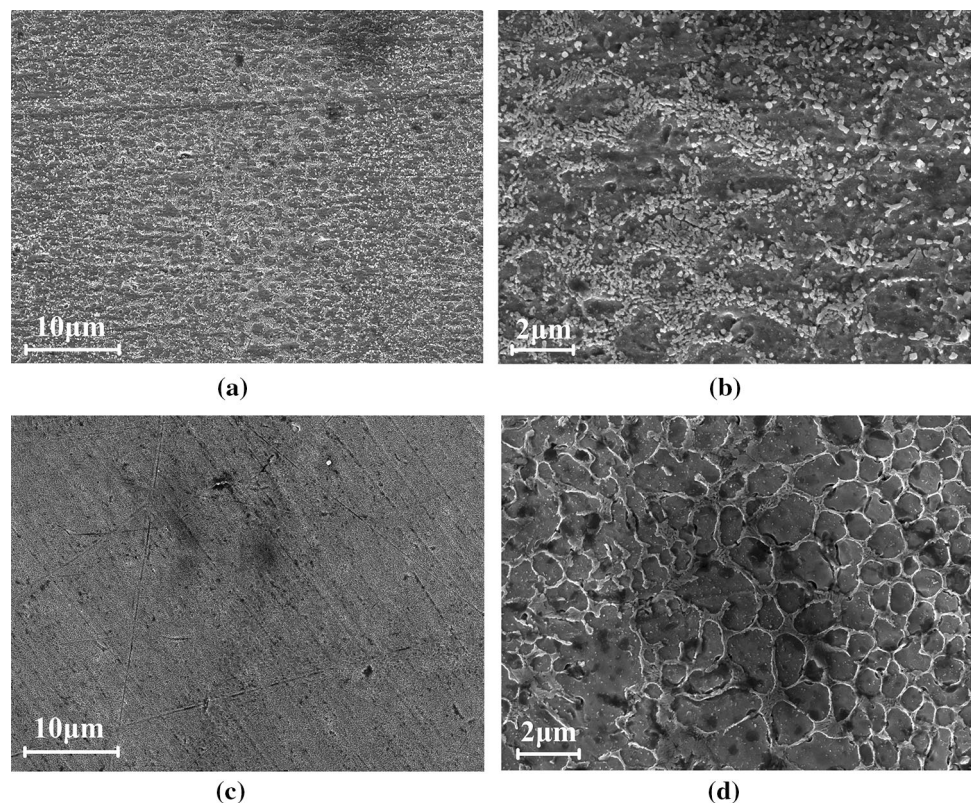
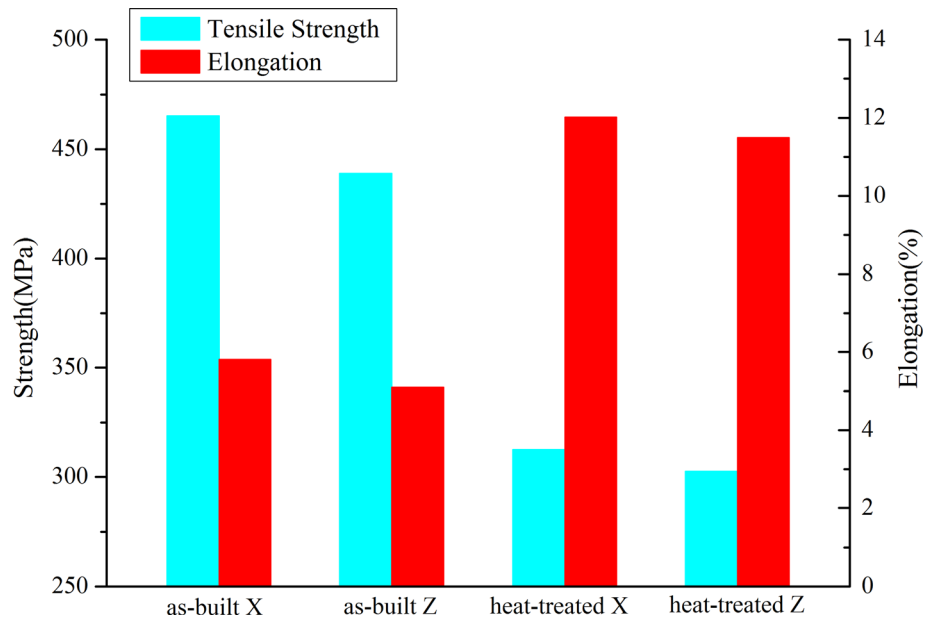


**Figure 10** Mechanical properties of as-built and heat-treated AlSi10Mg.



specimen between the X- and Z-directions (3.17%) was less than half that of the as-built AlSi10Mg specimen (6.45%). Therefore, the T6-like heat treatment increases the isotropy of AlSi10Mg fabricated by SLM.

### Microhardness of as-built and heat-treated AlSi10Mg

The hardness at selected points on the XZ and XY planes of as-built and heat-treated AlSi10Mg specimens was measured at 20 °C. The results are presented in Fig. 11. The Vickers hardness of the XY surface of the as-built AlSi10Mg specimen of 129.4–130.0 exceeds that of its XZ surface of 122.5–126. The hardness of the as-built AlSi10Mg specimen is similar to the Vickers hardness of forged 6061-T6 (128.2).

The average hardness of the heat-treated AlSi10Mg specimen of 107 is comparatively low; however, the hardness of its XY and XZ planes is approximately equal. This is consistent with the results of the tensile tests; that is, T6-like heat treatment reduces the anisotropy of AlSi10Mg fabricated by SLM.

### Thermal expansion of as-built and heat-treated AlSi10Mg

Plots of the linear expansion coefficients of as-built and heat-treated AlSi10Mg specimens as functions of the temperature are shown in Fig. 12. The linear

expansion coefficients of the as-built AlSi10Mg specimen in the X- and Z-directions tend to increase with increasing temperature. Under the same temperature conditions, the linear expansion coefficients of the as-built AlSi10Mg specimen in the two directions differ. In the range of 20–30 °C, the average linear expansion coefficients in the X- and Z- directions of  $21.79 \times 10^{-6} \text{ K}^{-1}$  and  $20.96 \times 10^{-6} \text{ K}^{-1}$ , respectively, differ by  $0.83 \times 10^{-6} \text{ K}^{-1}$ . The linear expansion coefficient in the X-direction exceeds that in the Z-direction. Similarly, the linear expansion coefficients of the heat-treated AlSi10Mg specimen in the X- and Z-directions tend to increase with increasing temperature; however, the linear expansion coefficients of the heat-treated AlSi10Mg specimen are lower than those of the as-built AlSi10Mg specimen. The linear expansion coefficients of the heat-treated AlSi10Mg specimen in the X- and Z-directions are similar. In the range of 20–30 °C, the average linear expansion coefficients in the X- and Z-directions of  $20.85 \times 10^{-6} \text{ K}^{-1}$  and  $20.92 \times 10^{-6} \text{ K}^{-1}$ , respectively, differ by only  $0.07 \times 10^{-6} \text{ K}^{-1}$ . The difference in the average linear expansion coefficients decreases from 3.96 to 0.33%, which confirms that the anisotropy of AlSi10Mg fabricated by SLM is reduced by T6-like heat treatment.



**Figure 11** Microhardness of as-built and heat-treated AlSi10Mg.

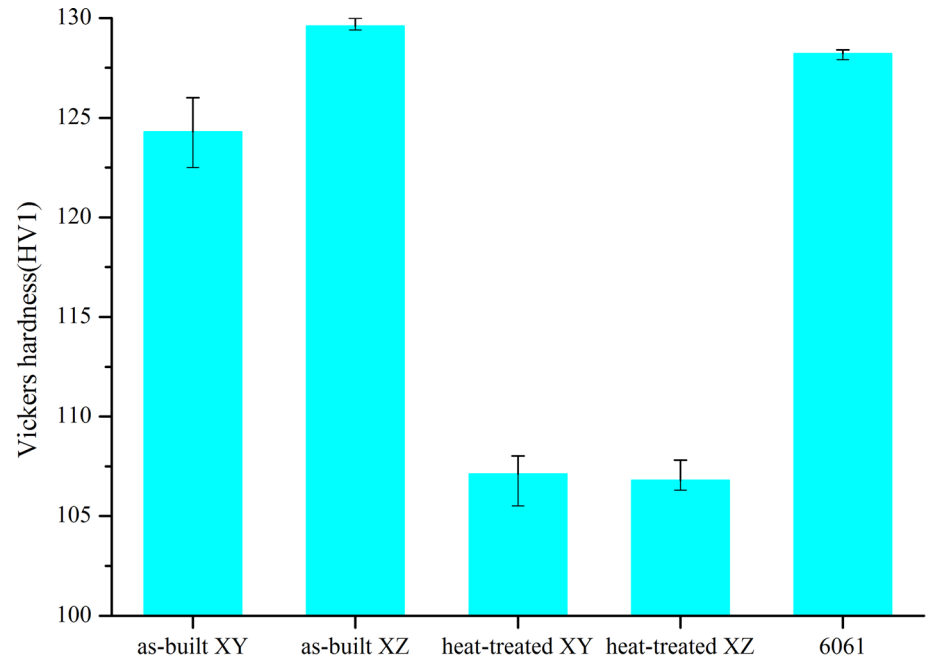
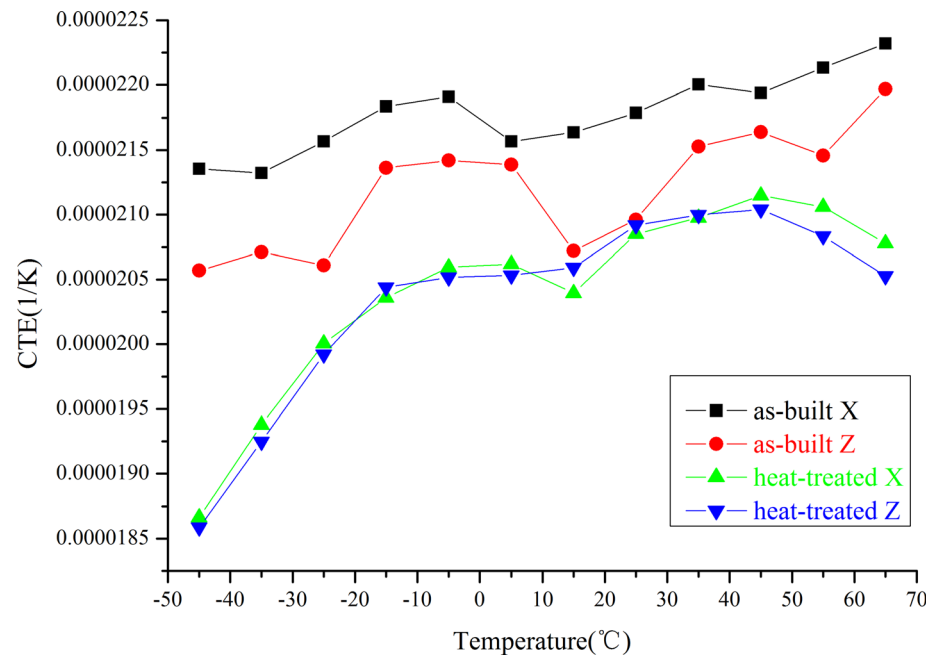


**Figure 12** Thermal expansion coefficients of as-built and heat-treated AlSi10Mg.



### Preparation of an additively manufactured mirror

These studies confirm that T6-like heat treatment effectively reduces the anisotropy of AlSi10Mg fabricated by SLM. To investigate the practical implications of this reduction in anisotropy, an additively manufactured mirror substrate consisting of AlSi10Mg was subjected to T6-like heat treatment.

The fabrication of the additively manufactured mirror substrate involved the following steps [30]:

- (1) Mirror fabrication: fabrication of a mirror substrate consisting of AlSi10Mg by SLM, leaving margins for processing.
- (2) Mirror processing: heat treatment of the substrate and subsequent machining of the mirror blank (substrate).

- (3) Single-point diamond turning (SPDT): processing of the mirror blank to reduce surface roughness and enhance surface accuracy.

The diameter of the additively manufactured mirror is 80 mm, and the interior is composed of traditional triangular lightweight structural units, as shown in Fig. 13a. Each side of the triangular units features a circular air hole to connect the triangular voids to the exterior through process holes on the boundary. The thickness of the inner walls of the mirror substrate is 2 mm to obtain a good balance between structural stability and low weight. The additively manufactured mirror, shown in Fig. 13b, was fabricated by SLM.

Owing to the SPDT of the mirror blank, the RMS of its surface accuracy is better than  $1/10\lambda$  ( $\lambda = 632.8$  nm), and the surface roughness is less than 10 nm. To test the stability of the additively manufactured mirror, it was subjected to repeated thermal cycling (3 cycles) between  $-55$  and  $70$  °C. The surface accuracy of the mirror was investigated before and after thermal cycling. The surface accuracy is illustrated in Fig. 14. The RMS of the surface accuracy of the additively manufactured mirror after thermal cycling remains  $0.095\lambda$  ( $\lambda = 632.8$  nm). Within the allowable margin of error, the stability of the surface accuracy of the mirror is good, which demonstrates that the heat-treated mirror substrate consisting of AlSi10Mg is dimensionally stable.

## Conclusions

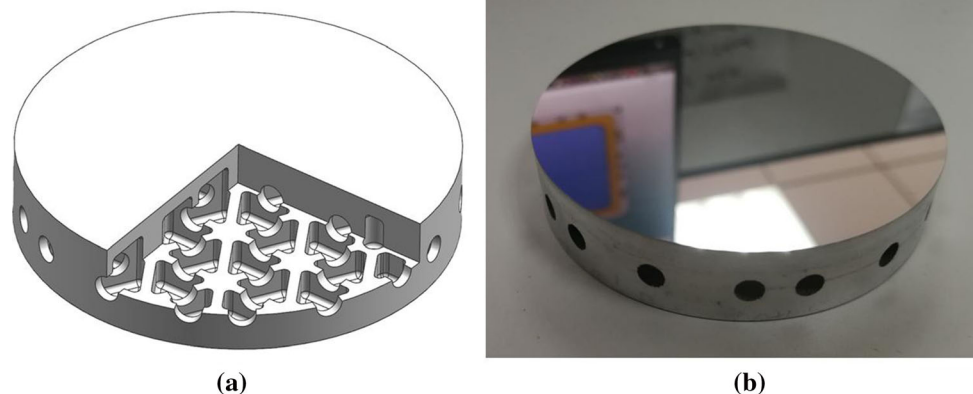
In this study, the influence of a T6-like heat treatment process on the structure and properties of AlSi10Mg fabricated by SLM was studied. The microstructures

and elemental distribution of as-built and heat-treated AlSi10Mg specimens were analyzed. In addition, their tensile strength, elongation, microhardness, and the coefficients of thermal expansion were compared. The main findings of this study are:

- (1) In the as-built AlSi10Mg specimen, precipitated eutectic Si phases form a network within the  $\alpha$ -Al matrix. The Si particle size in the remelted and heat-affected zones is larger than that in the center of the melt channel. In the heat-treated AlSi10Mg specimen, Si phases no longer form a network within the  $\alpha$ -Al matrix; instead, Si grains are uniformly distributed in the  $\alpha$ -Al matrix.
- (2) The mechanical properties of AlSi10Mg fabricated by SLM are affected by heat treatment. This is owing to the precipitation, aggregation, and growth of Si grains as well as the growth of crystal grains during heat treatment. The tensile strength of the as-built AlSi10Mg specimen is 467.1 MPa, but its elongation is only 5.8%. In contrast, the tensile strength and elongation of the heat-treated AlSi10Mg specimen are lower and higher (by a factor of 2) than those of the as-built AlSi10Mg specimen. The tensile strength, elongation, hardness, and thermal expansion of the heat-treated AlSi10Mg specimen are similar in the build (Z) and scan (X) directions.

Although the T6-like heat treatment of AlSi10Mg fabricated by SLM impairs its hardness and tensile strength, it improves its elongation and reduces its anisotropy. Moreover, the surface accuracy of a heat-treated, additively manufactured mirror consisting of AlSi10Mg is stable. This study is expected to inform the realization of additively manufactured mirrors—

**Figure 13** Additively manufactured mirror; **a** diagram of lightweight substrate and **b** image of the mirror after SPDT.





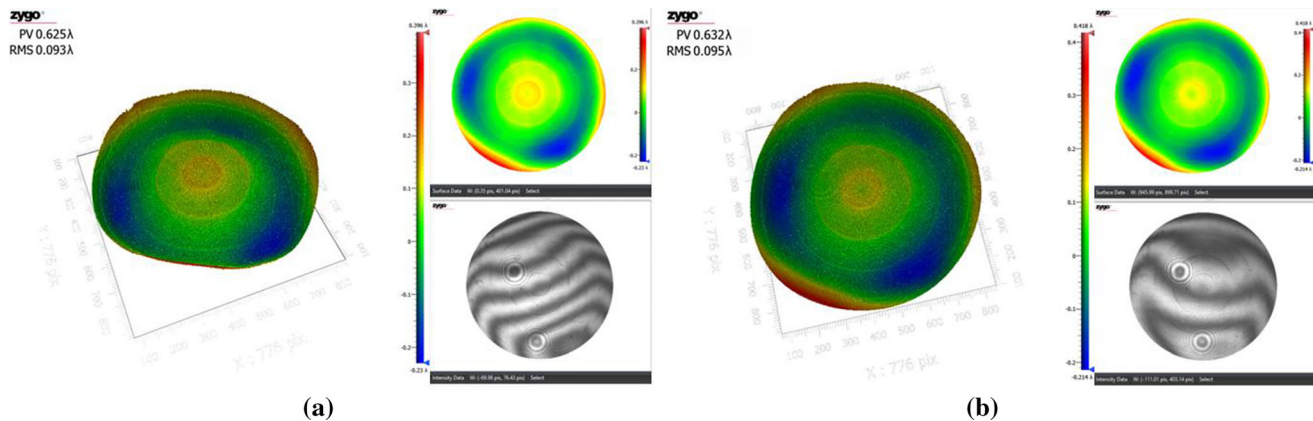


**Figure 14** Mirror surface accuracy **a** before and **b** after thermal cycling.

with stable surface accuracy—suitable for application in extreme environments.

## Acknowledgements

This research was funded by The National Key Research and Development Program of China; this research was funded by Key laboratory of Airborne Optical Imaging and Measurement, grant number HCKF-201912HJ03. The authors are thankful for the support provided by the Key Laboratory of Airborne Optical Imaging and Measurement, Changchun Institute of Optics, Fine Mechanics and Physics, Chinese Academy of Sciences.

## Author Contributions

ST was involved in conceptualization, methodology, software, resources, data curation, writing—original draft preparation, writing—review and editing, visualization; YD contributed to validation; ST and YW were involved in investigation; WL contributed to supervision; PJ was involved in project administration; HW, PJ and YD contributed to funding acquisition. All authors have read and agreed to the published version of the manuscript.

## Declarations

**Conflict of interest** The authors declare that there is no conflict of interest.

## References

- [1] Sweeney M, Acreman M, Vettese T, Myatt R, Thompson M (2015) Application and testing of additive manufacturing for mirrors and precision structures. Proc. SPIE 9574, Material technologies and applications to optics, structures, components, and sub-systems II, 957406. <https://doi.org/10.1117/12.2189202>
- [2] Olakanmi EO, Cochrane RF, Dalgarno KW (2015) A review on selective laser sintering/melting (SLS/SLM) of aluminium alloy powders: processing, microstructure, and properties. Prog Mater Sci 74:401–477. <https://doi.org/10.1016/j.pmatsci.2015.03.002>
- [3] Roulet M, Atkins C, Hugot E, Lemared S, Lombardo S, Ferrari M (2018) 3D printing for astronomical mirrors. 3D printed optics and additive photonic manufacturing. Proc. SPIE 10675, 3D printed optics and additive photonic manufacturing, 1067504. <https://doi.org/10.1117/12.2306836>
- [4] Atkins C, Feldman C, Brooks D, et al (2018) Topological design of lightweight additively manufactured mirrors for space. Proc. SPIE 10706, Advances in optical and mechanical technologies for telescopes and instrumentation III, 107060I. <https://doi.org/10.1117/12.2313353>
- [5] Herzog H, Segal J, Smith J, et al (2015) Optical fabrication of lightweighted 3D printed mirrors. Proc. SPIE 9573, Optomechanical engineering, 957308. <https://doi.org/10.1117/12.2188197>
- [6] Mercelis P, Kruth J (2006) Residual stresses in selective laser sintering and selective laser melting. Rapid Prototype 12(5):254–265. <https://doi.org/10.1108/13552540610707013>
- [7] Ullah R, Akmal JS, Laakso SVA, Niemi E (2020) Anisotropy of additively manufactured AlSi10Mg: threads and surface integrity. Int J Adv Manuf Technol

- 107(9):3645–3662. <https://doi.org/10.1007/s00170-020-05243-8>
- [8] Segebade E, Gerstenmeyer M, Dietrich S, Zanger F, Schulze V (2019) Influence of anisotropy of additively manufactured AlSi10Mg parts on chip formation during orthogonal cutting. *Procedia CIRP* 82:113–118. <https://doi.org/10.1016/j.procir.2019.04.043>
- [9] Girelli L, Tocci M, Gelfi M, Pola A (2019) Study of heat treatment parameters for additively manufactured AlSi10Mg in comparison with corresponding cast alloy. *Mater Sci Eng A* 739:317–328. <https://doi.org/10.1016/j.msea.2018.10.026>
- [10] Majeed A, Zhang Y, Lv J, Peng T, Atta Z, Ahmed A (2020) Investigation of T4 and T6 heat treatment influences on relative density and porosity of AlSi10Mg alloy components manufactured by SLM. *Comput Ind Eng* 139:106194. <https://doi.org/10.1016/j.cie.2019.106194>
- [11] Rosenthal I, Stern A, Frage N (2014) Microstructure and mechanical properties of AlSi10Mg parts produced by the laser beam additive manufacturing (AM) technology. *Metallogr Microstruct Anal* 3(6):448–453. <https://doi.org/10.1007/s13632-014-0168-y>
- [12] Salmi A, Atzeni E, Iuliano L, Galati M (2017) Experimental analysis of residual stresses on AlSi10Mg parts produced by means of selective laser melting (SLM). *Procedia CIRP* 62:458–463. <https://doi.org/10.1016/j.procir.2016.06.030>
- [13] DebRoy T, Wei HL, Zuback JS, Mukherjee T, Elmer JW, Milewski JO, Beese AM, Wilson-Heid A, De A, Zhang W (2018) Additive manufacturing of metallic components—process, structure and properties. *Prog Mater Sci* 92:112–224. <https://doi.org/10.1016/j.pmatsci.2017.10.001>
- [14] Majeed A, Ahmed A, Salam A, Sheikh MZ (2019) Surface quality improvement by parameters analysis, optimization and heat treatment of AlSi10Mg parts manufactured by SLM additive manufacturing. *Int J Lightweight Mater Manuf* 2(4):288–295. <https://doi.org/10.1016/j.ijlmm.2019.08.001>
- [15] Sol T, Hayun S, Noiman D, Tiferet E, Yeheskel O, Tevet O (2018) Nondestructive ultrasonic evaluation of additively manufactured AlSi10Mg samples. *Addit Manuf* 22:700–707. <https://doi.org/10.1016/j.addma.2018.06.016>
- [16] Strumza E, Hayun S, Barzilai S, Finkelstein Y, David RB, Yeheskel O (2019) In situ detection of thermally induced porosity in additively manufactured and sintered objects. *J Mater Sci* 54(11):8665–8674. <https://doi.org/10.1007/s10853-019-03452-5>
- [17] Gushev MN, Sridharan N, Thompson Z, Terrani KA, Babu SS (2018) Influence of hot isostatic pressing on the performance of aluminum alloy fabricated by ultrasonic additive manufacturing. *Scripta Mater* 145:33–36. <https://doi.org/10.1016/j.scriptamat.2017.10.004>
- [18] Cao S, Zou Y, Lim CVS, Wu X (2021) Review of laser powder bed fusion (LPBF) fabricated Ti-6Al-4V: process, post-process, treatment, microstructure, and property. *Light Adv Manuf* 2:20. <https://doi.org/10.37188/lam.2021.020>
- [19] Hitzler L, Charles A, Öchsner A (2016) The influence of post-heat-treatments on the tensile strength and surface hardness of selective laser melted AlSi10Mg. *Defect and diffusion forum*. Trans Tech Publ Ltd 370:171–176. <https://doi.org/10.4028/www.scientific.net/DDF.370.171>
- [20] Aboulkhair NT, Maskery I, Tuck C, Ashcroft I, Everitt NM (2016) The microstructure and mechanical properties of selectively laser melted AlSi10Mg: the effect of a conventional T6-like heat treatment. *Mater Sci Eng A* 667:139–146. <https://doi.org/10.1016/j.msea.2016.04.092>
- [21] Trevisan F, Calignano F, Lorusso M, Pakkanen J, Aversa A, Ambrosio EP, Lombardi M, Fino P, Manfredi D (2017) On the selective laser melting (SLM) of the AlSi10Mg alloy: process, microstructure, and mechanical properties. *Materials (Basel)* 10(1):76. <https://doi.org/10.3390/ma10010076>
- [22] Tan S, Ding Y, Xu Y, Shi L (2020) Design and fabrication of additively manufactured aluminum mirrors. *Opt Eng* 59(1):013103. <https://doi.org/10.1117/1.OE.59.1.013103>
- [23] Han X, Kang N, Jiao J, Wang C (2019) Research for surface characteristics of aluminum mirrors made by laser additive manufacturing. *Proc. SPIE* 11333, AOPC 2019: advanced laser materials and laser technology, 113331I. <https://doi.org/10.1117/12.2548108>
- [24] Strumza E, Yeheskel O, Hayun S (2019) The effect of texture on the anisotropy of thermophysical properties of additively manufactured AlSi10Mg. *Addit Manuf* 29:100762. <https://doi.org/10.1016/j.addma.2019.06.013>
- [25] Brandl E, Heckenberger U, Holzinger V, Buchbinder D (2012) Additive manufactured AlSi10Mg samples using selective laser melting (SLM): microstructure, high cycle fatigue, and fracture behavior. *Mater Des* 34:159–169. <https://doi.org/10.1016/j.matdes.2011.07.067>
- [26] Wang L, Wang S, Hong X (2018) Pulsed SLM-manufactured AlSi10Mg Alloy: mechanical properties and microstructural effects of designed laser energy densities. *J Manuf Process* 35:492–499. <https://doi.org/10.1016/j.jmapro.2018.09.007>
- [27] Kempen K, Thijs L, Van Humbeeck J, Kruth J-P (2012) Mechanical properties of AlSi10Mg produced by selective laser melting. *Phys Procedia* 39:439–446. <https://doi.org/10.1016/j.phpro.2012.10.059>
- [28] Read N, Wang W, Essa K, Attallah MM (2015) Selective laser melting of AlSi10Mg alloy: process optimisation and mechanical properties development. *Mater Des* 65:417–424. <https://doi.org/10.1016/j.matdes.2014.09.044>
- [29] Newswander T, Crowther B, Gubbels G, Senden R (2013) Aluminum alloy AA-6061 and RSA-6061 heat treatment for



large mirror applications. Proc. SPIE 8837, Material technologies and applications to optics, structures, components, and sub-systems, 883704. <https://doi.org/10.1117/12.2024369>

- [30] Hilpert E, Hartung J, Risse S, Eberhardt R, Tünnermann A (2018) Precision manufacturing of a lightweight mirror body

made by selective laser melting. *Precis Eng* 53:310–317. [h  
https://doi.org/10.1016/j.precisioneng.2018.04.013](https://doi.org/10.1016/j.precisioneng.2018.04.013)

**Publisher's Note** Springer Nature remains neutral with regard to jurisdictional claims in published maps and institutional affiliations.